Second-harmonic generation in arrays of spherical particles

W. Luis Mochán and Jesús A. Maytorena
Centro de Ciencias Físicas, Universidad Nacional Autónoma de México, Apartado Postal 48-3, 62251 Cuernavaca, Morelos, México

Bernardo S. Mendoza
Centro de Investigaciones en Optica, Apartado Postal 948-1, 37000 León, Guanajuato, México

Vera L. Brudny
Departamento de Física, Facultad de Ciencias Exactas y Naturales, Universidad de Buenos Aires, Buenos Aires, Argentina
(Received 14 November 2002; revised manuscript received 31 March 2003; published 19 August 2003)

We calculate the optical second harmonic (SH) radiation generated by small spheres made up of a homogeneous centrosymmetric material illuminated by inhomogeneous transverse and/or longitudinal electromagnetic fields. We obtain expressions for the hyperpolarizabilities of the particles in terms of the multipolar bulk susceptibilities and dipolar surface susceptibilities of their constitutive material. We employ the resulting response functions to obtain the nonlinear susceptibilities of a composite medium made up of an array of such particles and to calculate the radiation patterns and the efficiency of SH generation from the bulk and the edge of thin composite films illuminated by finite beams. Each sphere has comparable dipolar and quadrupolar contributions to the nonlinear radiation, and the composite has comparable bulk and edge contributions which interfere among themselves yielding nontrivial radiation and polarization patterns. We present numerical results for Si spheres and we compare our results with recent experiments.

DOI: 10.1103/PhysRevB.68.085318 PACS number(s): 78.66.−w, 73.20.Mf, 42.65.−k, 03.50.De

I. INTRODUCTION

Optical second harmonic generation (SHG) in centrosymmetric systems has proved to be a useful spectroscopic probe of surfaces, as the bulk contribution is strongly suppressed due to the symmetry.[1] As opposed to other surface techniques, SHG permits the observation of surfaces out of ultrahigh vacuum and in many different ambients. For instance, it may be employed to study buried interfaces. Although most of the theoretical and experimental work has been performed on flat surfaces,[2,3] other shapes have also been explored, most notably, spherical particles.[4] Recently, SHG was employed to explore a thin composite layer made up of Si spherical nanocrystallites embedded within a SiO_2 matrix.[5] It was found that the signal came mainly from the nanoparticles, not from the matrix, and that its strength diminished by an order of magnitude when the buried Si/SiO_2 interfaces were passivated with hydrogen, thus demonstrating the sensitivity of SHG to the condition of the surface of the particles and its usefulness for studying novel electronic devices. However, experiment showed that the transmitted intensity displayed a peak along the forward direction and with a very narrow angular aperture. This result was unexpected, as previous theory[6] indicated that the radiation produced by a single sphere illuminated by a plane wave vanishes identically along the forward direction, as has been corroborated through experiments with suspended colloidal particles.[7,8]

The theory of Dadap *et al.*[6] mentioned above was developed for spheres illuminated by a plane electromagnetic wave. However, the nonlinear response of the particles actually depends on the nature of the exciting field, as shown by Brudny *et al.*[9] which obtained alternative results for the case of a longitudinal exciting field. In general, the polarizing field is neither of a pure longitudinal character nor is it a simple plane wave. For example, within a composite, the electric field has longitudinal short range spatial fluctuations[10] besides the transverse macroscopic field, and the latter is not necessarily a plane wave. Thus, in the first part of this paper, we generalize the theories above to calculate the quadratic nonlinear response functions of a single small nonmagnetic centrosymmetric sphere illuminated by an arbitrary nonhomogeneous electromagnetic field, constrained only by the absence of external charges within the sphere. Afterward, we employ the resulting hyperpolarizabilities to calculate the macroscopic second order susceptibilities of a composite. Finally, we calculate the SHG from a thin homogeneous slab of this composite illuminated by a focused Gaussian beam, and from an inhomogeneous composite with a density gradient. We find similar bulk and surface contributions to the signal produced by a single sphere. Its dipolar and quadrupolar contributions are also similar, and their relative strength depends on the spatial variation of the polarizing field. As expected, a plane wave produces no coherent SHG exactly along the forward direction, but a finite sized beam produces a nontrivial radiation pattern around the forward direction when it illuminates a homogeneous composite film. The density gradient at the edge of the sample produces a signal that may be larger than that coming from the interior and has different patterns and polarizations, depending on the direction of the incoming electric field with respect to the edge.

The paper is organized as follows: In Sec. II we develop the theory for the nonlinear response of a small single sphere. In Sec. III we obtain the macroscopic nonlinear susceptibilities of a homogeneous composite and we employ them to calculate the SHG of a thin film illuminated by a Gaussian beam, and in Sec. IV we take account of the inho-

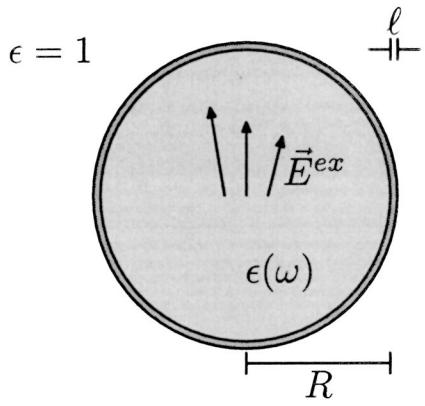

FIG. 1. Nonmagnetic sphere of radius R with dielectric function $\epsilon(\omega)$ within a vacuum, being acted upon by an inhomogeneous electric field $\vec{E}^{\rm ex}$. The selvedge of width ℓ is shown as a dark shell.

mogeneity of the density to calculate the radiation from the edge of the film. Within a continuous dipolium model,[11] in Sec. V we calculate the response functions and the radiation patterns and intensities corresponding to Si nanospheres, and we compare our results with experiment. Finally, Sec. VI is devoted to a discussion of our results and to conclusions. The details of the derivation presented in Sec. II are included in Appendix A, and the results are compared with those in the literature in Appendix B.

II. NONLINEAR RESPONSE OF A SINGLE SPHERE

We first consider a single homogenous, local, isotropic, centrosymmetric, nonmagnetic sphere of radius R centered at the origin, with a linear response characterized by a dielectric function $\epsilon(\omega)$. For simplicity we consider that outside the sphere there is only vacuum (Fig. 1).

The sphere is acted upon by an inhomogeneous external field $\vec{E}^{\rm ex}(\vec{r})$, oscillating at frequency ω. We assume that the scale of spatial variation of this polarizing field is much larger than R. Due to quadratic nonlinear optical processes, the sphere may acquire a dipole moment $\vec{p}^{(2)}$ and a quadrupole moment $\vec{\vec{Q}}^{(2)}$ in response to the external field. The symmetry of the sphere implies that, to lowest order in the field gradient, $\vec{p}^{(2)}$ has to be constructed from a combination of only $\vec{E}^{\rm ex}(0)$ and $\nabla\vec{E}^{\rm ex}(0)$ yielding a vector. The only posibility is

$$\vec{p}^{(2)}=\gamma^{\rho}\vec{E}^{\rm ex}(0)\nabla\cdot\vec{E}^{\rm ex}(0)+\gamma^{e}\vec{E}^{\rm ex}(0)\cdot\nabla\vec{E}^{\rm ex}(0)+\gamma^{m}\vec{E}^{\rm ex}(0)\times[(\nabla\times\vec{E}^{\rm ex}(0)]. \quad (1)$$

Similarly, $\vec{\vec{Q}}^{(2)}$ should be written as a traceless, symmetric tensor quadratic in $\vec{E}^{\rm ex}(0)$,[9]

$$\vec{\vec{Q}}^{(2)}=\gamma^{q}\left(\vec{E}^{\rm ex}(0)\vec{E}^{\rm ex}(0)-\frac{1}{3}[E^{\rm ex}(0)]^2\vec{\vec{1}}\right). \quad (2)$$

Related to $\vec{\vec{Q}}^{(2)}$, we will also calculate the scalar second moment $\tilde{Q}^{(2)}$ of the nonlinear induced charge distribution, given by

$$\tilde{Q}^{(2)}=\tilde{\gamma}^{q}[E^{\rm ex}(0)]^2. \quad (3)$$

Finally, there is no quadratic magnetization, as no combination of only $\vec{E}^{\rm ex}$ and $\nabla\vec{E}^{\rm ex}$ can yield an axial vector. As the sphere is small, we need not consider further multipolar moments nor higher order spatial derivatives of the field. The purpose of the present section is the calculation of the nonlinear response functions γ^{ν} to lowest order in R, where $\gamma^{\nu}=\gamma^{e},\gamma^{m},\gamma^{q}$, and $\tilde{\gamma}^{q}$.

Assuming that R is small enough, we linearize the field within the sphere as

$$\vec{E}^{\rm ex}(\vec{r})=\vec{E}^{0}+\vec{r}\cdot\nabla\vec{E}^{0}+O(r^2). \quad (4)$$

Making an expansion in irreducible tensors,[12] we write

$$E_i^{\rm ex}(\vec{r})=E_i^{0}+\frac{1}{3}(\nabla\cdot\vec{E}^{0})r_i+\frac{1}{2}[(\nabla\times\vec{E}^{0})\times\vec{r}]_i+\frac{1}{2}\left(\partial_i E_j^{0}+\partial_j E_i^{0}-\frac{2}{3}\nabla\cdot\vec{E}^{0}\delta_{ij}\right)r_j, \quad (5)$$

and employing Maxwell's equations,

$$\vec{E}^{\rm ex}(\vec{r})=\vec{E}^{0}+\frac{4\pi}{3}\rho^{0}\vec{r}+\frac{iq}{2}\vec{B}^{0}\times\vec{r}+\frac{1}{2}\vec{\vec{C}}^{0}\cdot\vec{r}, \quad (6)$$

where ρ^0 is the external charge density, $\vec{B}^0$ the external magnetic field, $\vec{\vec{C}}^0$ is a second order symmetric traceless tensor and $q=\omega/c$ is the characteristic wave number for the incident field.

In the following we will make the reasonable assumption that there is no external charge within the sphere, $\rho^0=0$, so that we disregard γ^{ρ}. We notice that the first and third term on the right hand side of Eq. (6) are irrotational and may be derived from a scalar potential with angular momenta $l=1$ and 2 respectively, while the second term is solenoidal. Thus, the self-consistent screened linear field $\vec{E}$ within the sphere is given by

$$\vec{E}(\vec{r})=L_{11}\vec{E}^{0}+\frac{iq}{2}\vec{B}^{0}\times\vec{r}+\frac{1}{2}L_{21}\vec{\vec{C}}^{0}\cdot\vec{r}, \quad (7)$$

where L_{lw} are the screening factors for potentials with angular momentum l and frequency $w\omega$,

$$L_{lw}=\frac{2l+1}{l\epsilon_w+l+1}, \quad (8)$$

and we abbreviated $\epsilon_w\equiv\epsilon(w\omega)$, $w=1,2$. Notice that, as the sphere is nonmagnetic, the solenoidal contribution to the field remains unscreened.

Now we chose a particularly simple polarizing field, for which $\vec{E}^0=(0,0,E^0)$ points along the z direction, $\vec{B}^0=(B^0,0,0)$ points along the x direction, and $\vec{\vec{C}}^0=\mathrm{diag}(-1,-1,2)C^0/2$ produces a potential with cylindrical symmetry

along the z axis. The hyperpolarizabilities γ^{ν} obtained for these fields may afterwards be employed for the general case. Thus, we write

$$\vec{E}^{\rm ex}(\vec{r})=E^0\begin{pmatrix}0\\0\\1\end{pmatrix}+\frac{iq}{2}B^0\begin{pmatrix}0\\-z\\y\end{pmatrix}+\frac{1}{4}C^0\begin{pmatrix}-x\\-y\\2z\end{pmatrix} \tag{9}$$

and

$$\vec{E}(\vec{r})=L_{11}E^0\begin{pmatrix}0\\0\\1\end{pmatrix}+\frac{iq}{2}B^0\begin{pmatrix}0\\-z\\y\end{pmatrix}+\frac{1}{4}L_{21}C^0\begin{pmatrix}-x\\-y\\2z\end{pmatrix}, \tag{10}$$

so we may identify

$$\vec{E}^{\rm ex}(0)\cdot\nabla\vec{E}^{\rm ex}(0)=\frac{1}{2}(0,-iqE^0B^0,E^0C^0), \tag{11}$$

$$\vec{E}^{\rm ex}(0)\times[\nabla\times\vec{E}^{\rm ex}(0)]=(0,iqE^0B^0,0), \tag{12}$$

$$\nabla[\vec{E}^{\rm ex}(0)]^2=(0,iqE^0B^0,E^0C^0), \tag{13}$$

$$\vec{E}^{\rm ex}(0)\vec{E}^{\rm ex}(0)-\frac{1}{3}[E^{\rm ex}(0)]^2\overleftrightarrow{1}={\rm diag}(-1,-1,2)(E^0)^2/3, \tag{14}$$

and

$$[E^{\rm ex}(0)]^2=(E^0)^2, \tag{15}$$

with similar results for the screened field [Eq. (10)].

The macroscopic quadratic polarization $\vec{P}^b$ induced by the linear field within the bulk of a homogeneous isotropic medium may be written as[13]

$$\vec{P}^b(\vec{r})=\gamma\nabla E^2+\delta'\vec{E}\cdot\nabla\vec{E}, \tag{16}$$

where $\gamma(\omega)$ and $\delta'(\omega)$ are the bulk nonlinear response functions. Using Eq. (10) we write

$$\vec{P}^b=\frac{1}{2}[0,-iqL_{11}(\delta'-2\gamma)E^0B^0,L_{11}L_{21}(\delta'+2\gamma)E^0C^0]+O(r). \tag{17}$$

Besides the bulk polarization $\vec{P}^b$, there is a surface quadratic polarizarion $\vec{P}^s$ due to dipolarly allowed processes in a narrow selvedge of width ℓ where centrosymmetry is locally broken:

$$P_i^s=\chi_{ijk}^sF_jF_k. \tag{18}$$

Here $\chi_{ijk}^s=\chi_{ijk}^s(\vec{R},\omega)$ is the second order surface susceptibility at position $\vec{R}$. As in Refs. 9 and 11, we define this susceptibility as the response to the continuous field

$$\vec{F}(\vec{R})=\vec{D}_{\perp}(\vec{R})+\vec{E}_{\parallel}(\vec{R}), \tag{19}$$

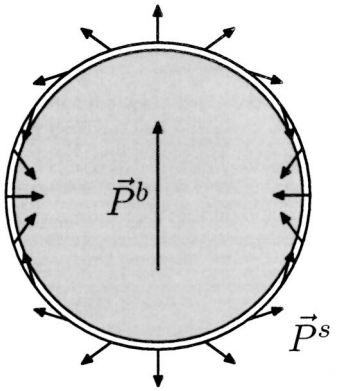

FIG. 2. Illustration of the nonlinear bulk polarization $\vec{P}^b$ and the surface polarization $\vec{P}^s$ located immediately outside the sphere.

constructed in terms of the displacement $\vec{D}$ and the electric $\vec{E}$ fields at the surface. The advantage of this definition is that it removes the ambiguities as to the position within the selvedge where the fields are to be evaluated. Also, we identify $\vec{P}^s$ as the total surface polarization, so that, in contrast to the bulk polarization $\vec{P}^b$, no further screening of $\vec{P}^s$ is necessary. This way, we also avoid the ambiguity as to where in the surface should the surface polarization be located; corresponding to $\vec{P}^s$ we place a singular polarization $\vec{P}^s\delta(r-R^+)$ in vacuum just outside of the sphere (Fig. 2).

Assuming that R is much larger than ℓ, we may safely consider the sphere to be locally flat. Notice that we have already stated that R is smaller than the spatial variation of the field, so in particular, it should be smaller than the optical wavelength λ. As ℓ is of the order of the screening depth, typically about an atomic distance, while λ is commonly two to three orders of magnitude larger, there is a range of sizes R for which the conditions $\ell\ll R\ll\lambda$ may be obeyed, such as for the 3–10-nm sized particles employed in the experiments of Ref. 5. Thus, we write

$$\chi_{ijk}^s=\chi^s\Big(\delta_{ir}\delta_{jr}\delta_{kr}\frac{a}{\epsilon_1^2}+[(1-\delta_{ir})(1-\delta_{jr})\delta_{kr}+(1-\delta_{ir})\delta_{jr}(1-\delta_{kr})]\frac{b}{\epsilon_1}+\delta_{ir}(1-\delta_{jr})(1-\delta_{kr})f\Big) \quad \text{(spherical)} \tag{20}$$

in the spherical coordinate basis $\hat{r},\hat{\theta},\hat{\varphi}$. Here, $a=a(\omega)$, $b=b(\omega)$ and $f=f(\omega)$ are the dimensionless functions which are commonly employed to parametrize the response of a flat homogeneous surface[14,15] that is isotropic within its plane,

$$\chi^s=\frac{(\epsilon_1-1)^2}{64\pi^2ne}, \tag{21}$$

n is the electronic density, and $-e$ is the electronic charge.

Integrating Eq. (17) over the bulk and Eq. (18) over the surface of the sphere, and accounting for linear screening at 2ω, we can obtain the total second order dipole moment. A similar process permits the calculation of the quadrupole moment. The results of these procedures are (see Appendix A)

$$\vec{p}^{(2)}=\frac{2\pi}{15}R^3L_{11}L_{12}\begin{pmatrix}0\\ -5iq[(\delta'-2\gamma)-2(\epsilon_2 f-b)\chi^s]E^0B^0\\ [5(\delta'+2\gamma)+2(2\epsilon_2 a+b+3\epsilon_2 f)\chi^s]L_{21}E^0C^0\end{pmatrix}, \tag{22}$$

$$Q_{zz}^{(2)}=\frac{32\pi}{15}R^3L_{11}^2L_{22}\chi^s(\epsilon_2 a+3b-\epsilon_2 f)(E^0)^2, \tag{23}$$

and

$$\tilde{Q}^s=\frac{8\pi}{3}R^3L_{11}^2\chi^s(a+2f)(E^0)^2. \tag{24}$$

Comparing Eq. (22) with Eq. (1) and employing Eqs. (11) and (12) we finally obtain the dipolar hiperpolarizabilities

$$\gamma^e=\frac{4\pi}{15}R^3L_{11}L_{12}L_{21}[5(\delta'+2\gamma)+2\chi^s(2\epsilon_2 a+b+3\epsilon_2 f)] \tag{25}$$

and

$$\gamma^m=\frac{2\pi}{15}R^3L_{11}L_{12}\{5[(\delta'+2\gamma)L_{21}-(\delta'-2\gamma)] +2\chi^s[(2\epsilon_2 a+b+3\epsilon_2 f)L_{21}-5(b-\epsilon_2 f)]\}. \tag{26}$$

Similarily, a comparison of Eq. (23) with Eqs. (2) and (14), and of Eq. (24) with Eqs. (3) and (15) yields

$$\gamma^q=\frac{16\pi}{5}R^3L_{11}^2L_{22}\chi^s(\epsilon_2 a+3b-\epsilon_2 f) \tag{27}$$

and

$$\tilde{\gamma}^q=\frac{8\pi}{3}R^3L_{11}^2\chi^s(a+2f). \tag{28}$$

A comparison (see Appendix B) of the expressions above with earlier work (Refs. 9, 6, and 16) shows that the present work corrects an oversight in Ref. 9 and extends its results to small spheres made up of isotropic, homogeneous, and centrosymmetric materials with arbitrary bulk and surface response functions γ, δ', a, b, and f and excited by a field with both longitudinal and transverse components. Our results are also a generalization of those of Refs. 6 and 16 to small nonmagnetic spheres immersed in vacuum and excited by a field which is not necessarily a plane wave.

In this section we have found expressions for the nonlinear response functions γ^ν of a single nanosphere in terms of the intrinsic response of the surface (a, b, f) and bulk (γ, δ') of flat semiinfinite homogeneous and isotropic materials. Thus, we may take advandtage of manifold models and measurements of those intrinsic response functions in order to obtain the nonlinear susceptibility of small particles.

III. NONLINEAR RESPONSE OF A COMPOSITE

In Sec. II we obtained the nonlinear response of a single sphere subject to an inhomogeneous field $\vec{E}^{\rm ex}$. In the present section we want to look at the response of a composite medium made up of such spheres, such as the nanocrystals that have been studied by Jiang *et al.*[5] In Ref. 5 a thin disordered array of Si spherical nanocrystals within a SiO_2 matrix was studied using SHG. The second harmonic radiation was found to be confined to a very narrow ($\approx 1°$) cone and peaked along the forward direction. At first sight, this result is intriguing: The first two contributions to the nonlinear dipole [Eq. (1)] of each sphere are null when the sphere is illuminated by a plane wave, while its quadrupole [Eq. (2)] would have an axis of cylindrical symmetry lying on the plane wavefront. Therefore, neither the second harmonic (SH) dipole nor the quadrupole moments of the sphere are expected to radiate along the forward direction.[6–8,16] Thus, it was suggested that the observed radiation originated from density, size and shape fluctuations.[5] However, the angular distribution of the radiation is inconsistent with the incoherent signal expected to arise from fluctuations.[5,9] Nevertheless, coherent SH radiation may appear when the sample is illuminated with a beam that has a finite waist, as actually employed in Ref. 5, since the in-plane inhomogeneity of the field amplitude might induce further nonlinear sources that might be able to radiate. In Fig. 3 we show schematically the SH dipole moments induced on a composite by a focused fundamental beam. Near the center of the beam, the dipoles point along the nominal propagation direction, and thus they cannot radiate into it. However, as the edge of the illuminated spot is approached, the fundamental amplitude decays, and the corresponding gradient tilts the nonlinear dipoles away from the forward direction. Thus, those dipoles may radiate close to the forward direction. Although the fields produced by dipoles located at opposite sides of the spot might cancel each other exactly along the forward direction, such cancelation is absent at small off-forward scattering angles, yielding a nontrivial intensity distribution. To illustrate this possibility, in this section we calculate the coherent SH radiated by a composite illuminated by a finite beam. We consider thus a system made up of a very narrow disordered array of small spheres distributed with a density $n_s(\vec{r})$ and illuminated by a finite beam. The place of the external field acting on a given sphere should be taken by the actual external field plus the field produced by other spheres. Thus, we should replace $\vec{E}^{\rm ex}$ by the local field $\vec{E}^{\rm loc}$. For simplicity, we further ignore the local field effect and identify $\vec{E}^{\rm loc}$ with the macroscopic field $\vec{E}^M$, which we denote in what follows

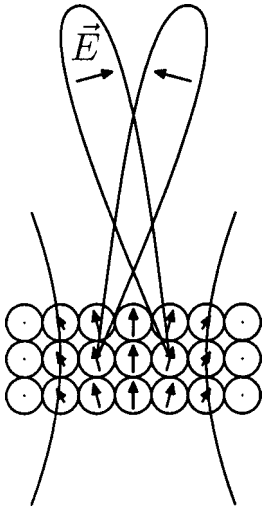

FIG. 3. Schematic representation of the SH dipole moments induced on a composite system illuminated by a focused beam. The SH field radiated at small off-normal directions is indicated, as well as the expected two lobed intensity distribution and the contributions of some dipoles to those lobes.

simply as $\vec{E}$ as it causes no confusion.

The macroscopic nonlinear polarization of the composite medium may be obtained from the nonlinear dipole and quadrupole of each of its component spheres,[17]

$$\vec{P}^{nl}=n_s\vec{p}^{(2)}-\frac{1}{6}\nabla\cdot n_s\vec{\vec{Q}}^{(2)}-\frac{1}{6}\nabla n_s\tilde{Q}^{(2)}, \tag{29}$$

where we include the scalar $\tilde{Q}$ as $\vec{\vec{Q}}$ is traceless. Within a homogeneous composite, $n_s(\vec{r})$ has a constant value n_b, and we employ Eqs. (1)–(3) to write

$$\vec{P}^{nl}=n_b\gamma^e\vec{E}\cdot\nabla\vec{E}+n_b\gamma^m\vec{E}\times(\nabla\times\vec{E})-n_b\frac{\gamma^q}{6}\vec{E}\cdot\nabla\vec{E}$$

$$+n_b\frac{\gamma^q-3\tilde{\gamma}^q}{18}\nabla E^2, \tag{30}$$

which becomes

$$\vec{P}^{nl}=\Gamma\nabla E^2+\Delta'\vec{E}\cdot\nabla\vec{E}, \tag{31}$$

after expanding the curl terms and eliminating the field divergence, where we introduced the response functions

$$\Gamma=\frac{n_b}{18}(9\gamma^m+\gamma^q-3\tilde{\gamma}^q) \tag{32}$$

and

$$\Delta'\equiv n_b(\gamma^e-\gamma^m-\gamma^q/6), \tag{33}$$

analogous to γ and δ' [Eq. (16)].

Now, we consider a thin sample of width l lying on the $z=0$ plane illuminated by a beam with a finite waist w_0, as in Ref. 5 (Fig. 4).

The unscreened SH vector potential $\vec{A}$ obeys

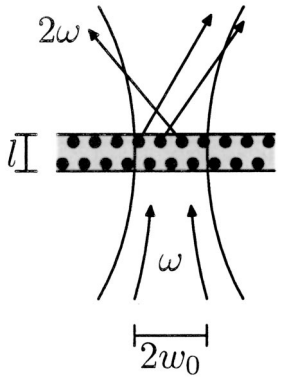

FIG. 4. A Gaussian beam is focused on a spot of radius w_0 on a thin composite film of width l giving rise to a SH scattered radiation.

$$\nabla^2\vec{A}^T+(2q)^2\vec{A}^T=-\frac{4\pi}{c}\vec{J}^T, \tag{34}$$

where the superscript T denotes the transverse projection of a vector field and $\vec{J}$ is the SH current

$$\vec{J}=\frac{\partial}{\partial t}\vec{P}^{nl}=-2i\omega\vec{P}^{nl}, \tag{35}$$

and we solve Eq. (34) to obtain

$$\vec{A}^T(\vec{r})=-2iq\int d^3r'\frac{e^{2iq|\vec{r}-\vec{r}'|}}{|\vec{r}-\vec{r}'|}[\vec{P}^{nl}(\vec{r}')]^T. \tag{36}$$

At large distances r from the illuminated spot we may perform the usual approximations $1/|\vec{r}-\vec{r}'|\approx 1/r$ and $e^{2iq|\vec{r}-\vec{r}'|}\approx e^{2iqr}e^{-2iq\hat{n}\cdot\vec{r}'}$ with $\hat{n}=(\sin\theta\cos\varphi,\sin\theta\sin\varphi,\cos\theta)$ a unit vector in the direction of $\vec{r}$, to obtain

$$\vec{A}^T(\vec{r})=-2iql\frac{e^{2iqr}}{r}(\vec{P}_K^{nl})^T, \tag{37}$$

where we assumed the film is much narrower than the wavelength, $ql\ll 1$, and we introduced the two-dimensional Fourier transform

$$\vec{P}_K^{nl}=\int d^2r_\parallel\vec{P}^{nl}(\vec{r}_\parallel,z=0)e^{-i\vec{K}\cdot\vec{r}_\parallel}, \tag{38}$$

with wave vector $\vec{K}=2q\hat{n}_\parallel$. Actually, much wider films may be considered, as long as phase matching effects are negligible, i.e., $ql\Delta n\ll 1$, with $\Delta n=n(2\omega)-n(\omega)$, and n is the index of refraction of the composite, and as long as beam divergence effects may also be neglected, i.e., $l\ll qw_0^2$. We now realize that the first term in Eq. (31) is purely longitudinal, so it cannot contribute to the radiated field. Thus, substituting into Eq. (37), we obtain the transverse potential

$$\vec{A}^T(\vec{r})=-2iql\frac{e^{2iqr}}{r}\Delta'(\vec{E}\cdot\nabla\vec{E})_K^T. \tag{39}$$

Using Eq. (39), we have reduced the problem of SH radiation from a thin composite film illuminated by a beam of finite cross section to that of the calculation of the in-plane Fourier transform of the nonlinear driving term $\vec{E}\cdot\nabla\vec{E}$.

To proceed, we assume that at $z=0$ the driving field $\vec{E}$ is given by the waist of a Gaussian beam and we assume that its width w_0 is much larger than the wavelength, so that the beam is paraxial around the nominal propagation direction z. Thus, we can ignore the small variations of order K/q in its polarization direction, and we can take a linearly polarized beam of the form

$$\vec{E}(\vec{r}_\parallel,0)=E_0 e^{-r_\parallel^2/w_0^2}\hat{x}, \tag{40}$$

where $\hat{x}$ is the unit vector in the x direction. In this case,

$$\vec{E}\cdot\nabla\vec{E}=-2\frac{E_0^2 x}{w_0^2}e^{-2r_\parallel^2/w_0^2}\hat{x} \tag{41}$$

is also linearly polarized along $\hat{x}$. Since we can consider x to be a transverse direction, normal to the nominal propagation axis z, we approximate $(\vec{E}\cdot\nabla\vec{E})^T\approx\vec{E}\cdot\nabla\vec{E}$, with the Fourier transform

$$(\vec{E}\cdot\nabla\vec{E})_K^T=\frac{i\pi}{4}K_x w_0^2 e^{-K^2w_0^2/8}E_0^2\hat{x}. \tag{42}$$

We substitute Eq. (42) into Eq. (39) to obtain the vector potential

$$\vec{A}^T(\vec{r})=\pi q^2 w_0^2 l\,\theta\cos\varphi e^{-q^2w_0^2\theta^2/2}\frac{e^{2iqr}}{r}\Delta' E_0^2\hat{x}, \tag{43}$$

where we wrote the wavevector in terms of the scattering direction and further assumed $\sin\theta\approx\theta$.

The radiated electric field $\vec{E}^r=2iq\vec{A}^T$ is immediatelly obtained from the potential [Eq. (43)], and from it we obtain Poynting's vector $\vec{S}=c|E^r|^2\hat{n}/8\pi$, the SH radiated intensity per unit solid angle into direction $\hat{n}$, $dI(\hat{n})/d\Omega=r^2\vec{S}(r\hat{n})\cdot\hat{n}$ and the differential efficiency of SH generation,

$$\frac{d\mathcal{E}}{d\Omega}\equiv\frac{1}{\mathcal{P}^2}\frac{dI}{d\Omega}, \tag{44}$$

given by

$$\frac{d\mathcal{E}}{d\Omega}=\frac{2}{\pi}(qw_0)^4\theta^2\cos^2\varphi e^{-q^2w_0^2\theta^2}\mathcal{E}, \tag{45}$$

where $\mathcal{P}$ is the incoming power,

$$\mathcal{P}=\frac{c}{8\pi}\int d^2r_\parallel|E(\vec{r}_\parallel,0)|^2=\frac{cw_0^2}{16}|E_0|^2, \tag{46}$$

and $\mathcal{E}$ is the integrated efficiency over the whole solid angle:

$$\mathcal{E}\equiv\frac{1}{\mathcal{P}^2}\int d\Omega\frac{dI}{d\Omega}=\frac{64\pi^2}{c}\frac{(ql)^2}{w_0^4}|\Delta'|^2. \tag{47}$$

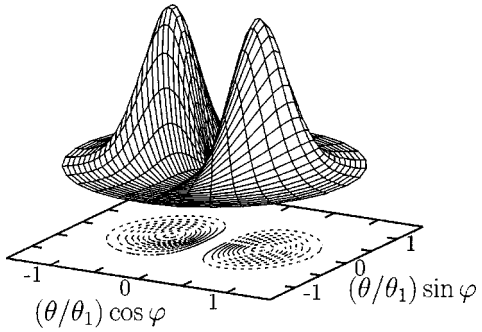

FIG. 5. SH intensity vs angular position of the detector for a disordered array of spheres illuminated by a Gaussian beam of width w_0 and frequency $\omega=qc$.

The radiated pattern obtained from Eq. (45) is shown in Fig. 5. Notice that there is no radiation along the forward direction, but there is a strong nonlinear signal along two lobes very close to the forward direction, displaced along the incoming polarization direction $\varphi=0$ by an angle $\pm\theta_2=\pm 1/(qw_0)$. The angular displacement $\theta_2=\theta_1/2=\theta_2^*/\sqrt{2}$ where θ_1 and θ_2^* are the beam divergence half-angles of the fundamental beam and of the SH field that would have been generated by a homogeneous non-centrosymmetric material, such as the quartz plates usually employed as a reference in SH experiments. We remark that the characteristic angles θ_1 and θ_2^* are defined in terms of the angular decay of the fundamental and SH far field *amplitudes*.[18] More directly observable are the corresponding quantities defined in terms of the angular decay of the fundamental and SH *intensities*, or equivalently, by the second moment of the angular distribution of the intensities, which are $\sqrt{2}$ times smaller.

We notice that the efficiency grows as the square of the thickness l of the system, since we assumed it to be very thin. It decreases as the inverse fourth power of the size of the illuminated spot, and for a fixed spot size and out of resonance, it grows as the square of the frequency. On the other hand, if the diffraction angle θ_1 is kept constant, the efficiency scales as its fourth power and as the sixth power of frequency. The order of magnitude of $\mathcal{E}$ may be estimated from Eqs. (20), (21), (25), (26), (27), (28), (33), and (47). Far from resonance, the hypolarizabilities γ^ν are of order $R^3\chi^s$ [Eqs. (25), (26), (27), and (28)], and χ^s is of order $10^{-3}/ne$. The electronic density n of a solid is typically of order $10/a_B^3$ where a_B is Bohr radius. Thus, from Eq. (33), $\Delta'\sim 10^{-2}f_b a_B^3/e$, where $f_b=4\pi n_b R^3/3$ is the filling fraction of the spheres. Substituting in Eq. (47) and writing the result in terms of $\theta_1=2/qw_0$, we finally obtain

$$\mathcal{E}=10^{-2}\zeta(qa_B)^4(ql)^2 f_b^2\theta_1^4\frac{1}{e^2/a_B}\frac{1}{c/a_B}$$
$$\approx 10^{-4}\zeta(qa_B)^4(ql)^2 f_b^2\theta_1^4\ \mathrm{W}^{-1}, \tag{48}$$

where ζ is a pure number which we expect to be of order unity, though it may vary by a couple of orders of magnitude due to the high powers of dimensionless numbers which appear implicitly in Eq. (47). The reasonable choice qa_B

$\approx 10^{-2}$, $ql \approx 1$, $f_b \approx 10^{-1}$, and $\theta_1 \approx 1° \approx 2\times 10^{-2}$ yields an efficiency $\mathcal{E} \approx 10^{-24}$ W^{-1}. For thicker composites, for which ql is larger than order 1, phase matching effects might have to be accounted for. Qualitatively, this may be accomplished simply by replacing l^2 in the previous equations by the phase mismatch factor, i.e.,

$$l^2 \rightarrow |\sin(ql\Delta n)/(q\Delta n)|^2. \tag{49}$$

Additional changes would be necessary for very thick samples with $l \approx q w_0^2$ or larger, for which the divergence of the fundamental and SH beams within the sample have to be accounted for. In the experiments of Jiang *et al.* described earlier[5] $l \approx 10/q$ was not so large as to produce phase mismatch effects and the other parameters were close to those mentioned above. On the other hand, about 100–300 SHG 3.1-eV photons were detected per second from a sample illuminated by 2.5×10^5 100–200 fs, 1-μJ pulses each second,[19] yielding the measured efficiency $\mathcal{E} \approx 10^{-23}$ W^{-1}, in good agreement with the estimation above.

The ubiquitous randomness within composites yields necessarily some incoherent radiation. Thus, it is instructive to estimate the efficiency of the incoherent SHG $\mathcal{E}_{\rm inc}$ and to compare it with its coherent counterpart $\mathcal{E}$ [Eq. (48)]. As the dipolar and quadrupolar radiation produced by a single sphere are similar, we estimate the intensity of the SH signal produced by an individual sphere through Larmor's formula $\mathcal{P}_1^{(2)} \sim c(2q)^4 (p^{(2)})^2/3 \sim 10cq^6(\chi^s)^2 R^6 E_0^4/3$, where we used Eq. (1) and we estimated $\gamma^\nu \sim \chi^s R^3$ and $E_0 \nabla E_0 \sim q E_0^2$. Multiplying by the number of illuminated spheres $\sim n_s l w_0^2$ and dividing by the square of the incident power Eq. (46), we obtain the incoherent efficiency

$$\mathcal{E}_{\rm inc} \sim f_b (q a_B)^4 \frac{q^2 l R^3}{w_0^2} \frac{1}{c/a_B} \frac{1}{e^2/a_B}, \tag{50}$$

where we employed the estimate for χ^s given above, so that

$$\frac{\mathcal{E}_{\rm inc}}{\mathcal{E}} \sim 10^1 \frac{(qR)^3 (q w_0)^2}{(ql) f_B}. \tag{51}$$

Substituting the parameters corresponding to the experiment of Jiang *et al.* (Ref. 5) mentioned above, we obtain that the coherent and incoherent contributions have comparable SH efficiency. However, the incoherent radiation is distributed over a wide solid angle, according to a superposition of dipolar and quadrupolar radiation patterns,[9] while the coherent radiation has a very narrow distribution close to the forward direction (Fig. 5) and, thus, it has a much larger intensity. On the other hand, the dependence of the incoherent signal on f_b and R differs[20] from that of the coherent signal, and for diluted samples such as suspensions, the incoherent radiation may dominate.[7,8,20]

IV. NONLINEAR RESPONSE AT THE EDGE OF THE COMPOSITE

Another intriguing observation was reported in Ref. 5 regarding the intensity of the SH signal as the fundamental beam was scanned laterally through the sample. The observed SH intensity as the beam crossed the edge of the composite was about an order of magnitude larger than the signal from well within the composite, instead of interpolating smoothly between the signal from the interior and the practically inexistent signal from the exterior, as could have been naively expected. Furthermore, the signal displayed strong oscillations close to the edge. Thus, in this section we concentrate our attention on the calculation of the SH radiation from the lateral edge of a thin composite made of small spheres, such as that considered in the previous section (see Fig. 6).

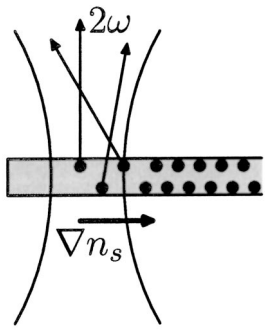

FIG. 6. A Gaussian beam is focused on the edge of a thin composite, as that in Fig. 4, producing SH radiation (light arrows). The gradient of the density of spheres ∇n_s close to the edge is indicated (heavy arrow).

Accounting for the variation of the density $n_s \equiv n_b \xi(x,y)$ across the illuminated spot, from Eq. (29) we obtain

$$\vec{P}^{nl} = \Delta' \xi \vec{E} \cdot \nabla \vec{E} + \Gamma \nabla(\xi E^2) - n_b \frac{\gamma^m}{2} E^2 \nabla \xi - n_b \frac{\gamma^q}{6} \vec{E} \vec{E} \cdot \nabla \xi, \tag{52}$$

instead of Eq. (31), where ξ is a function which varies from 0 outside the composite to its bulk value 1 within. Without loss of generality we take the edge along the y axis, so that $\xi = \xi(x)$, and we write $\nabla n_s = n_b (d\xi/dx)\hat{x} \equiv n_b \xi'(x)\hat{x}$. Then, Eq. (52) reduces to

$$\vec{P}^{nl} = \Delta' \xi \vec{E} \cdot \nabla \vec{E} + \Gamma \nabla(\xi E^2) + \Upsilon_\nu \xi'(x) \hat{x} E^2, \tag{53}$$

where Υ_ν depends on whether the external field $\vec{E}$ points in the direction parallel ($\nu = \|$) or perpendicular ($\nu = \perp$) to the gradient of n_s,

$$\Upsilon_\| = -n_b \left(\frac{\gamma^m}{2} + \frac{\gamma^q}{6} \right), \quad \Upsilon_\perp = -n_b \frac{\gamma^m}{2}. \tag{54}$$

The far field is now given by

$$\vec{A}^T(\vec{r}) = -2iql \frac{e^{2iqr}}{r} (\Delta' \xi \vec{E} \cdot \nabla \vec{E} + \Upsilon_\nu \xi' \hat{x} E^2)_K^T \tag{55}$$

instead of Eq. (39). To proceed, we chose a smooth density profile and we assume that its spatial scale of variation is larger than w_0, so we approximate it by a linear profile

$$\xi(x) = \xi_0 + x/L, \tag{56}$$

with ξ_0 representing the relative density at the center of the beam, which we take without loss of generality at $x=0$, and L is a distance of the order of the width of the edge. Substituting Eq. (56) into Eq. (55), performing the Fourier transform under the assumption of a small illuminated spot ($w_0 < L$), and calculating the resulting radiation pattern, we finally obtain

$$\frac{d\mathcal{E}_{\parallel}}{d\Omega}=\frac{8}{\pi}\mathcal{E}_b\frac{e^{-4\theta^2/\theta_1^2}}{\theta_1^2}\left|\frac{2\theta}{\theta_1}\cos\varphi+i\frac{w_0}{\xi_0 L}\times\left(\frac{1}{2}-2\frac{\theta^2}{\theta_1^2}\cos^2\varphi-\frac{\Upsilon_{\parallel}}{\Delta'}\right)\right|^2, \tag{57}$$

$$\mathcal{E}_{\parallel}=\mathcal{E}_b\left[1+\left(\frac{w_0}{\xi_0 L}\right)^2\left(\frac{3}{8}+2\left|\frac{\Upsilon_{\parallel}}{\Delta'}\right|^2-\mathrm{Re}\frac{\Upsilon_{\parallel}}{\Delta'}\right)\right], \tag{58}$$

$$\frac{d\mathcal{E}_{\perp}}{d\Omega}=\frac{8}{\pi}\mathcal{E}_b\frac{e^{-4\theta^2/\theta_1^2}}{\theta_1^2}\left[\left|\frac{2\theta}{\theta_1}\sin\varphi-i\frac{w_0}{\xi_0 L}\frac{\theta^2}{\theta_1^2}\sin 2\varphi\right|^2+\left|\frac{\Upsilon_{\perp}}{\Delta'}\right|^2\left(\frac{w_0}{\xi_0 L}\right)^2\right], \tag{59}$$

$$\mathcal{E}_{\perp}=\mathcal{E}_b\left[1+\left(\frac{w_0}{\xi_0 L}\right)^2\left(\frac{1}{8}+2\left|\frac{\Upsilon_{\perp}}{\Delta'}\right|^2\right)\right], \tag{60}$$

where $\mathcal{E}_b$ is the total efficiency of a homogeneous film [Eq. (47)] but evaluated at the nominal density $n_b\xi_0$ at the center of the illuminating beam, i.e., $\mathcal{E}_b=\xi_0^2\mathcal{E}$. Here, $d\mathcal{E}_\nu/d\Omega$ and $\mathcal{E}_\nu$ denote the differential and total SHG efficiencies for the case in which the incoming polarization points along the direction $\nu=\parallel,\perp$. More detailed information may be obtained by analyzing the outgoing beam with a linear polarizer. In this case we obtain

$$\frac{d\mathcal{E}_{\parallel\parallel}}{d\Omega}=\frac{d\mathcal{E}_{\parallel}}{d\Omega}, \tag{61}$$

$$\mathcal{E}_{\parallel\parallel}=\mathcal{E}_{\parallel}, \tag{62}$$

$$\frac{d\mathcal{E}_{\perp\parallel}}{d\Omega}=0, \tag{63}$$

$$\mathcal{E}_{\perp\parallel}=0, \tag{64}$$

$$\frac{d\mathcal{E}_{\parallel\perp}}{d\Omega}=\frac{8}{\pi}\mathcal{E}_b\frac{e^{-4\theta^2/\theta_1^2}}{\theta_1^2}\left|\frac{\Upsilon_{\perp}}{\Delta'}\right|^2\left(\frac{w_0}{\xi_0 L}\right)^2, \tag{65}$$

$$\mathcal{E}_{\parallel\perp}=2\mathcal{E}_b\left(\frac{w_0}{\xi_0 L}\right)^2\left|\frac{\Upsilon_{\perp}}{\Delta'}\right|^2, \tag{66}$$

$$\frac{d\mathcal{E}_{\perp\perp}}{d\Omega}=\frac{8}{\pi}\mathcal{E}_b\frac{e^{-4\theta^2/\theta_1^2}}{\theta_1^2}\left|\frac{2\theta}{\theta_1}\sin\varphi-i\frac{w_0}{\xi_0 L}\frac{\theta^2}{\theta_1^2}\sin 2\varphi\right|^2, \tag{67}$$

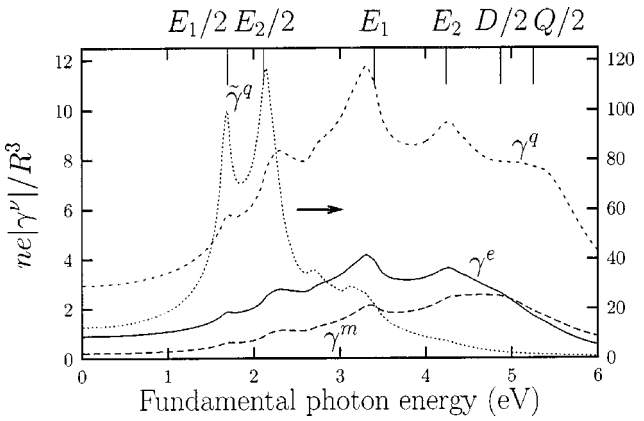

FIG. 7. Absolute value of the nonlinear response functions $|\gamma^\nu|$, where $\gamma^\nu=\gamma^e,\gamma^m,\gamma^q$, and $\tilde{\gamma}^q$ for a single Si nanosphere. The labels E_1 and E_2 denote the critical points of Si, $E_1/2$ and $E_2/2$ denote their subharmonics, and $D/2$ and $Q/2$ denote the subharmonics of the dipolar and quadrupolar resonances, for which $\mathrm{Re}\,\epsilon_2=-2$ and $-3/2$.

$$\mathcal{E}_{\perp\perp}=\mathcal{E}_b\left[1+\frac{1}{8}\left(\frac{w_0}{\xi_0 L}\right)^2\right], \tag{68}$$

where $d\mathcal{E}_{\mu\nu}/d\Omega$ and $\mathcal{E}_{\mu\nu}$ denote the differential and total efficiencies, with μ and ν denoting the outgoing and the incoming polarizations respectively.

V. RESULTS FOR SI NANOCRYSTALLITES

As Ref. 5 presents experimental results for Si nanospheres, in this section we apply to them some of our previous results. For simplicity, we calculate the surface and bulk nonlinear response functions of Si from its linear dielectric function[21] using the continuous dipolium model.[11] In Fig. 7 we show the nonlinear response of a single Si nanosphere, obtained from Eqs. (B4)–(B8).

Some structures visible in this figure are inherited from the linear bulk responses ϵ_1 and ϵ_2 and thus appear at the fundamental or at the subharmonic frequencies of the critical points of the Si joint density of states. Further structures are due to the nonlinear surface response a.[9,11] The resonances of

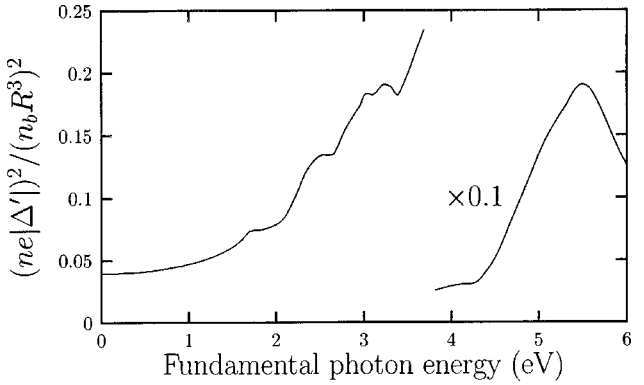

FIG. 8. Squared absolute value $|\Delta'|^2$ of the bulk nonlinear response of a homogeneous composite made up of spherical Si inclusions.

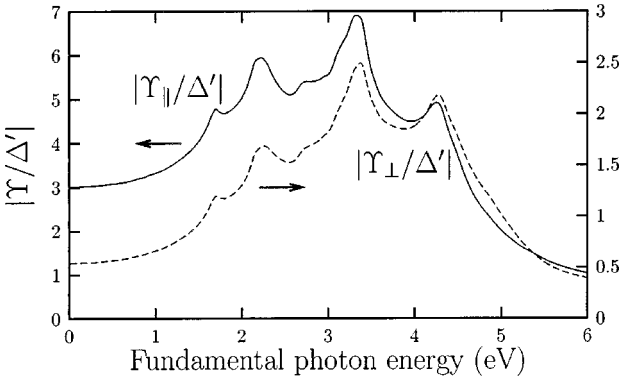

FIG. 9. Absolute value Υ_ν/Δ' of the quotient between the edge and the bulk response functions at the edge of a composite made of Si nanospheres for two directions of the incoming polarization, parallel ($\nu=\parallel$) and perpendicular($\nu=\perp$) to the density gradient ∇n_s.

the screening factors L_{l2} are too damped due to the finite imaginary part of ϵ_2 and the resonances of L_{l1} are outside of the spectral region shown in Fig. 7.

In Fig. 8 we show the bulk response Δ' calculated for a homogeneous composite made of n_b Si nanospheres per unit volume, calculated by substituting the nonlinear response of each Si particle, shown in Fig. 7, into Eq. (33). We notice that only its squared magnitude $|\Delta'|^2$ enters the differential and total SHG efficiencies [Eqs. (45) and (47)], and that the composite response Γ does not contribute. Fig. 8 shows that the efficiency increases almost monotonically up to about 5.5 eV, but has many features corresponding roughly to those displayed in Fig. 7. However, γ^ν are complex quantities and they interfere among themselves, leading to a richer structure in Fig. 8.

As shown by Eqs. (57)–(68), the differential and total SH efficiencies at the edge of a thin composite layer depend on the nominal efficiency of a homogeneous composite $\mathcal{E}_b$ and on the quotients $\Upsilon_\parallel/\Delta'$ and $\Upsilon_\perp/\Delta'$, which together with the relative widths w_0 and L of the beam and the edge control the relative contribution from the field and the density gradients. Figure 9 illustrates the frequency dependence of these relative contributions.

In Fig. 10 we show the SH radiation patterns from the edge of the composite film. The incoming energy $\hbar\omega = 1.55$ eV and polarization $\parallel$ are the same as in the experiment of Jiang *et al.*[5] We assumed the nominal beam focused at the middle of the edge, with a nominal density $n_s = 0.5n_b$. We notice that for a wide edge, or equivalently, for a thin beam, the differential efficiency is the same as the two lobbed radiation pattern of Fig. 5 for a homogeneous film (left panel). However, for a wider beam or a thinner edge a new contribution coming from the gradient ∇n_s of the density appears, filling the minimum between the two lobes (middle panel). Furthermore, the interference between the bulk-like and edge signals produces an asymmetry between both lobes; the lobe that leans towards ∇n_s is smaller. As could be expected from Fig. 9, the degree of asymmetry depends on the frequency. Already for $w_0/L \approx 0.1$ the gradient contribution dominates and the two-lobed structure is almost lost (right panel), although a slight asymmetry is still visible. In this case the peak is about twice as high as those for the homogeneous film.

In Fig. 11 we show the corresponding results but for polarization perpendicular to ∇n_s, i.e., along the edge. As $\Upsilon_\perp < \Upsilon_\parallel$ at $\hbar\omega = 1.55$ eV, higher values of w_0/L are required before the gradient contribution becomes visible. In this case, the two lobes are rotated with respect to those of Fig. 10 and retain their symmetry. The gradient and the bulk-like contributions are polarized along and normal to ∇n_s respectively. Thus the relatively small gradient contribution in Fig. 11 may be isolated by analyzing the outgoing beam with a linear polarizer. The polarized radiation pattern $d\mathcal{E}_{\parallel\perp}/d\Omega$ is a simple Gaussian [Eq. (65)] for all values of w_0/L.

VI. DISCUSSION AND CONCLUSIONS

In this paper we first obtained the quadratic optical response of a single centrosymmetric nonmagnetic isotropic sphere illuminated by an inhomogeneous electromagnetic field. As we did not make assumptions about the nature of the polarizing field, our results may be employed for both transverse and longitudinal exciting fields. Thus they consti-

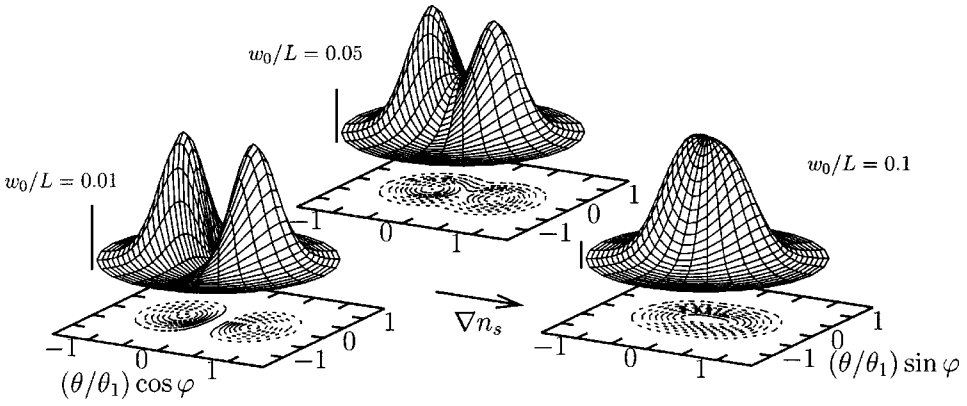

FIG. 10. SH radiation patterns $d\mathcal{E}_\parallel/d\Omega$ from the edge of a composite thin film made up of Si nanospheres for various values of the beam width w_0 and the edge size L, $w_0/L = 0.01$, 0.05, and 0.1. The energy of the incoming photons is $\hbar\omega = 1.55$ eV and we chose the nominal density at half the bulk value $n_s = 0.5n_b$. For reference, small vertical bars corresponding to the same fixed height $0.5\mathcal{E}_b$ are shown in each panel. The arrow indicates the direction of the density gradient.

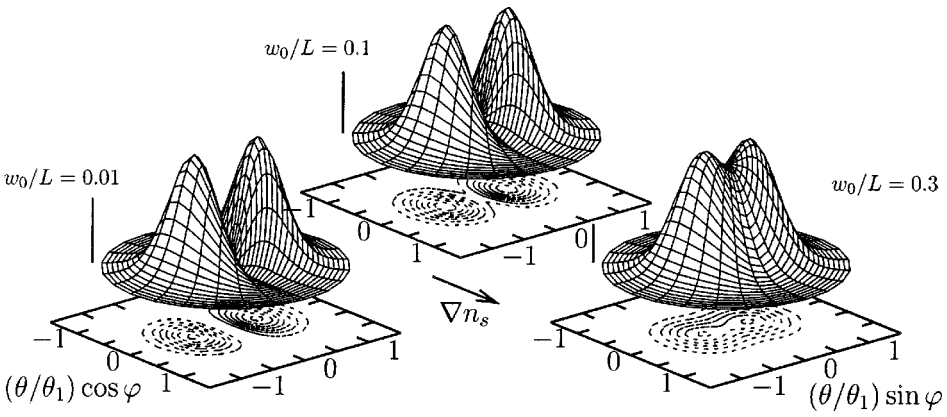

FIG. 11. SH radiation patterns $d\mathcal{E}_\perp/d\Omega$ as in Fig. 10 but for a polarization perpendicular to the density gradient ∇n_s. The vertical bar references have the same size as in Fig. 10.

tute a generalization of previous works.[9,6,16] The hyperpolarizabilities γ^e, γ^m, γ^q, and $\tilde{\gamma}^q$ were calculated to lowest order (R^3) in the size of the particles and were written in terms of their bulk and surface second order susceptibilities under the assumption that the curvature was small enough that the surface could be considered locally flat.

As has been discussed previously,[6] each individual sphere is unable to radiate in the forward direction when illuminated by a plane wave. However, the experimental observation of a very narrow SH peak in the forward direction from composite films made up of spherical Si nanocrystals embedded in SiO_2 was recently reported.[5] To understand its origin, we applied our results to the calculation of the response of composites illuminated by a focused Gaussian linearly polarized beam. We obtained that neither in this case can there be radiation exactly in the forward direction. However, the radiation pattern shows two narrow lobes displaced along the polarization direction by a small angle of the order of the diffraction-induced angular divergence of the linear far field. The forward peak reported experimentally for an array of Si nanospheres[5] may have been confused with one of these lobes.[19] We discussed the dependence of the SH differential and total efficiencies on parameters such as the width of the film, the density of inclusions, and the waist of the beam.

The experiment also showed that the signal may be enhanced at the lateral edge of finite films. Thus, we calculated the SH radiation produced at a non-homogeneous film. We found bulklike contributions and contributions due to the gradient of the inclusion density. The radiation patterns, the dependence on the input polarization, the output polarization directions, and the spectral features of both contributions differ in general, and they arise from different combinations of the individual sphere's response functions. These contributions may interfere among themselves, yielding nontrivial patterns which may be modified by changing the frequency, the waist of the illuminating beam, or the sharpeness of the edge. By analyzing the polarization of the outgoing beams gradient and bulk-like contributions may be separated, facilitating the analysis of the response functions. Calculations for a Si nanosphere composite within a simple dipolium model[11] agree qualitatively with the experimental observations.[5]

The solid-angle resolved SH patterns radiated by the bulk and edge we have calculated have not been explored experimentally yet. The bulk radiation of the composite depends on a single parameter Δ', which in turn depends, through the hyperpolarizabilities γ^ν, on the bulk and surface response functions δ', γ, a, b, and f, of an individual sphere. As the radiation from the edge involves different combinations Υ_ν of the above response functions, proper measurements might provide additional information to partially disentangle the separate contributions. We hope that this work will stimulate further experiments and theory.

ACKNOWLEDGMENTS

We are grateful to Michael Downer for showing us his results previous to publication and to him and to Tony Heinz for useful discussions. We acknowledge the support from DGAPA-UNAM under Grant Nos. IN110999 and IN117402 (W.L.M. and J.M.), from Conacyt under Grant No. 36033-E (B.M.), and from Fundación Antorchas (VLB). V.L.B. is also with CONICET, Argentina.

APPENDIX A: SECOND ORDER DIPOLE AND QUADRUPOLE MOMENTS OF A SPHERE

To obtain the surface polarization, we substitute Eqs. (10), (19), (20), and (21) into Eq. (18), leading to

$$\vec{P}^s=\chi^s\begin{pmatrix}(a\cos^2\theta+f\sin^2\theta)\\ -2b\sin\theta\cos\theta\\ 0\end{pmatrix}L_{11}^2(E^0)^2+\frac{1}{2}\chi^s\begin{pmatrix}[a\cos\theta(3\cos^2\theta-1)+3f\cos\theta\sin^2\theta]\\ b\sin\theta(1-6\cos^2\theta)\\ 0\end{pmatrix}L_{11}L_{21}RE^0C^0$$
$$+iq\chi^s\begin{pmatrix}f\sin\theta\sin\varphi\\ -b\cos\theta\sin\varphi\\ -b\cos^2\theta\cos\varphi\end{pmatrix}L_{11}RE^0B^0+O(R^2)\quad\text{(spherical)}. \tag{A1}$$

Now we calculate the dipole and quadrupole moments produced by the bulk $\vec{P}^b$ and surface $\vec{P}^s$ polarizations. Integrating Eq. (17) within the volume of the sphere we obtain the bulk contribution to the nonlinear dipole moment, given to lowest order in R by

$$\vec{p}^b=\frac{2\pi}{3}R^3L_{11}[0,-iq(\delta'-2\gamma)E^0B^0,L_{21}(\delta'+2\gamma)E^0C^0]. \tag{A2}$$

We notice that there is a contribution to $\vec{P}^s$ of order $O(R^0)$ so that even a constant external field induces a nonlinear polarization at the surface of the sphere due to the local loss of centrosymmetry. However, once we convert Eq. (A1) to Cartesian coordinates and integrate over the surface, it yields a null contribution to the total nonlinear dipole of the sphere, as the sphere is globally centrosymmetric. On the other hand, converting to Cartesian coordinates and integrating the second and third terms on the right hand side of Eq. (A1) yields a finite surface contribution to the nonlinear dipole

$$\vec{p}^s=\vec{p}^s_\parallel+\vec{p}^s_\perp, \tag{A3}$$

where

$$\vec{p}^s_\parallel=\frac{4\pi}{15}R^3\chi^sL_{11}\begin{pmatrix}0\\-5iqbE^0B^0\\bL_{21}E^0C^0\end{pmatrix} \tag{A4}$$

originates from the polarization $\vec{P}^s_\parallel$ parallel to the surface, and

$$\vec{p}^s_\perp=\frac{4\pi}{15}R^3\chi^sL_{11}\begin{pmatrix}0\\5iqfE^0B^0\\(2a+3f)L_{21}E^0C^0\end{pmatrix} \tag{A5}$$

from the polarization $\vec{P}^s_\perp$ perpendicular to the surface. Both contributions are proportional to the volume of the sphere and we neglect terms of higher order in R.

We now proceed to the calculation of the quadrupole moment:

$$\vec{\vec{Q}}=\int d^3r\rho(\vec{r})(3\vec{r}\vec{r}-r^2\vec{\vec{1}}). \tag{A6}$$

We write the density in terms of the polarization $\rho=-\nabla\cdot\vec{P}$, and we include in $\vec{P}$ the quadratic bulk contribution $\vec{P}^b$ [Eq. (17)] and the singular surface polarization $\vec{P}^s\delta(r-R^+)$ (Eq. (A1)). Integrating Eq. (A6) by parts we obtain a bulk contribution

$$\vec{\vec{Q}}^b=\int_V d^3r[3(\vec{P}^b\vec{r}+\vec{r}\vec{P}^b)-2\vec{P}^b\cdot\vec{r}\vec{\vec{1}}], \tag{A7}$$

and a surface contribution

$$\vec{\vec{Q}}^s=R^3\int d^2\Omega[3(\vec{P}^s\hat{r}+\hat{r}\vec{P}^s)-2\vec{P}^s\cdot\hat{r}\vec{\vec{1}}], \tag{A8}$$

where V denotes the volume of the sphere, and Ω is the solid angle. To lowest order, the bulk polarization is constant, leading to a bulk contribution $\vec{\vec{Q}}^b$ to quadrupole (A7) of order $O(R^4)$, which moreover vanishes from symmetry. The lowest order surface polarization is independent of R and yields a quadrupole of order R^3. From Eq. (A1), we notice that this term is independent of B^0 and C^0 and is produced only by the constant part of the external field $\vec{E}^0$. Thus, in the calculation of $\vec{\vec{Q}}^s$ we may assume cylindrical symmetry around the z axis and write $\vec{\vec{Q}}^s=\mathrm{diag}(-1,-1,2)Q^s_{zz}/2$. Substituting Eq. (A1) into Eq. (A8) and performing the integral, we obtain

$$Q^s_{zz}=Q^s_{zz\parallel}+Q^s_{zz\perp}, \tag{A9}$$

where

$$Q^s_{zz\parallel}=\frac{32\pi}{5}R^3L_{11}^2\chi^sb(E^0)^2 \tag{A10}$$

originates from $\vec{P}^s_\parallel$ and

$$Q^s_{zz\perp}=\frac{32\pi}{15}R^3L_{11}^2\chi^s(a-f)(E^0)^2 \tag{A11}$$

originates from $\vec{P}^s_\perp$.

Finally, we calculate the second moment of the quadratic induced charge

$$\tilde{Q}=\int d^3r\rho(\vec{r})r^2. \tag{A12}$$

As we did above, we write ρ in terms of the polarization and integrate by parts to obtain a bulk contribution,

$$\tilde{Q}^b=2\int d^3r\vec{P}^b\cdot\vec{r}, \tag{A13}$$

and a surface contribution,

$$\tilde{Q}^s=2R^3\int d^2\Omega\vec{P}^s\cdot\hat{r}, \tag{A14}$$

in analogy to Eqs. (A7) and (A8). As above, to order $O(R^3)$ there is no bulk contribution. The surface contribution,

$$\tilde{Q}^s=\frac{8\pi}{3}R^3L_{11}^2\chi^s(a+2f)(E^0)^2, \tag{A15}$$

may be obtained by substituting the first term on the right hand side of Eq. (A1) in Eq. (A14). The only finite contribution to Eq. (A15) originates from the perpendicular surface polarization $\vec{P}^s_\perp$.

To get the total multipole moments of the sphere we cannot simply add the bulk and surface contributions (A2), (A4), (A5), or (A10), (A11), as we have yet to account for the screening at 2ω of the fields produced by $\vec{P}^b$ and $\vec{P}^s$ within the bulk of the sphere. To this end we briefly follow Ref. 9. Since there is no magnetic moment induced and we assumed the sphere to be very small, in its immediate neighborhood

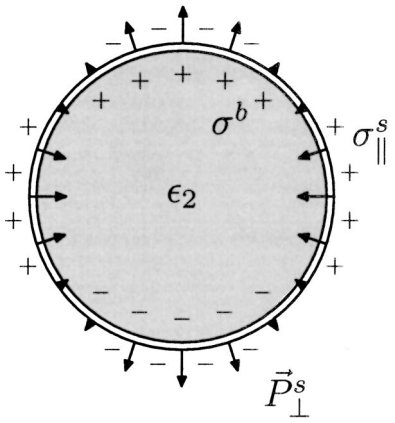

FIG. 12. Illustration of the surface polarization $P^s_\perp$, and the surface charge density σ^b and $\sigma^s_\parallel$ produced by the bulk polarization $\vec{P}^b$ and the surface polarization $\vec{P}^s_\parallel$, respectively. The figure corresponds qualitatively to Fig. 2. Due to screening, additional charges are induced at the boundary of the sphere with dielectric response ϵ_2, but they are not shown. There is no additional screening surface polarization.

we can neglect retardation and describe the selfconsistent field in terms of a quasistatic scalar potential ϕ. The equation obeyed by ϕ is

$$\nabla^2\phi=\begin{cases}-4\pi\rho^b/\epsilon_2 & \text{(inside)}\\ 0 & \text{(outside)},\end{cases} \tag{A16}$$

where the unscreened bulk charge density at 2ω, $\rho^b=-\nabla\cdot\vec{P}^b$, is divided by ϵ_2 to yield the screened charge density. The boundary conditions obeyed by ϕ are

$$\phi(R^+)-\phi(R^-)=4\pi P^s_\perp \tag{A17}$$

and

$$\frac{\partial}{\partial R}\phi(R^+)-\epsilon_2\frac{\partial}{\partial R}\phi(R^-)=-4\pi\sigma. \tag{A18}$$

Equation (A17) expresses the discontinuity of the potential due to a singular surface polarization, while Eq. (A18) expresses the discontinuity of the normal component of the field due to the surface charge $\sigma=\sigma^b+\sigma^s_\parallel$ which has a bulk originated contribution $\sigma^b=\vec{P}^b\cdot\hat{r}$ and a surface originated contribution $\sigma^s_\parallel=-\nabla_\parallel\cdot\vec{P}^s_\parallel$ produced by the parallel component of the surface polarization $\vec{P}^s$ (see Fig. 12).

As discussed above, $\vec{P}^s$ denotes the self-consistent surface polarization and therefore, there is no additional screening contribution to it. However, $\vec{P}^s$ may induce a field within the sphere, and this field may lead to an additional induced bulk polarization and to bulk and surface screening charges. These are accounted for by the factors ϵ_2 in Eqs. (A16) and (A18).

Now we expand all quantities in Eqs. (A16)–(A18) in terms of spherical harmonics $Y_{lm}(\theta,\varphi)$ as $\phi=\Sigma\phi_{lm}Y_{lm}$, $\rho^b=\Sigma\rho^b_{lm}Y_{lm}$, $P^s_\perp=\Sigma(P^s_\perp)_{lm}Y_{lm}$, etc. Since ρ^b contributes terms of at least order $O(R^4)$ to the dipolar moment $\vec{p}^{(2)}$ and $O(R^5)$ to the quadrupolar moment $Q^{(2)}$ and the second moment $\tilde{Q}^{(2)}$, in the following we will neglect it. Actually, it turns out that ρ^b is a constant so it has no contribution to the terms with $l\neq 0$, for which Eq. (A16) becomes Laplace's equation, with solution

$$\phi_{lm}(r)=\frac{4\pi}{2l+1}\times\begin{cases}F_{lm}r^l & \text{(inside)}\\ q_{lm}/r^{l+1} & \text{(outside)},\end{cases} \tag{A19}$$

where we identify q_{lm} with the spherical components of the multipolar moments.[22] The coefficients q_{lm} and F_{lm} are determined by boundary conditions (A17) and (A18), which become

$$\frac{q_{lm}}{R^{l+1}}-F_{lm}R^l=(2l+1)(P^s_\perp)_{lm}, \tag{A20}$$

and

$$(l+1)\frac{q_{lm}}{R^{l+2}}+l\epsilon_2F_{lm}R^{l-1}=(2l+1)(\sigma^b_{lm}+\sigma^s_{\parallel lm}), \tag{A21}$$

and yield

$$\begin{aligned}q_{lm}&=L_{l2}[(\sigma^b_{lm}+\sigma^s_{\parallel lm})R^{l+2}+l\epsilon_2(P^s_\perp)_{lm}R^{l+1}]\\&=q^b_{lm}+q^s_{\parallel lm}+q^s_{\perp lm},\end{aligned} \tag{A22}$$

with L_{l2} the screening factor (8) at the second harmonic for the angular momentum l. Here we have identified a bulk contribution $q^b_{lm}\propto\sigma^b\propto P^b$, a surface contribution originated in the tangential surface polarization $q^s_{\parallel lm}\propto\sigma^s_\parallel\propto P^s_\parallel$, and a surface contribution originated in the perpendicular polarization $q^s_{\perp lm}\propto P^s_\perp$.

Setting $\epsilon_2\to 1$, $L_{l2}\to 1$ in Eq. (A22) we obtain the unscreened multipolar moments, which are then simply compared to their screened counterparts, yielding

$$q^b_{lm}(\text{screened})=L_{l2}q^b_{lm}(\text{unscreened}), \tag{A23}$$

$$q^s_{\parallel lm}(\text{screened})=L_{l2}q^s_{\parallel lm}(\text{unscreened}), \tag{A24}$$

and

$$q^s_{\perp lm}(\text{screened})=L_{l2}\epsilon_2q^s_{\perp lm}(\text{unscreened}). \tag{A25}$$

Thus, the total dipole ($l=1$) and quadrupole ($l=2$) moments may be obtained from the unscreened moments obtained previously [Eqs. (A2), (A4), (A5), (A10), and (A11)] by multiplying by the screening factor L_{l2} at 2ω. Those multipoles that originate in the perpendicular surface polarization $P^s_\perp$ [Eqs. (A5) and (A11)] are to be further multiplied by ϵ_2.

After screening and adding the bulk [Eq. (A2)] and surface [Eqs. (A4) and (A5)] contributions, we obtain the total nonlinear dipole $\vec{p}^{(2)}$ induced in the sphere, given by Eq. (22). Similarly, we screen and add the contributions to the induced quadrupole [Eqs. (A10) and (A11)] to obtain the total quadrupole moment (23). Finally, we notice that $\tilde{Q}^s$ is determined only by the $l=0$ contribution to the normal polarization $(P^s_\perp)_{00}$, and that the field produced by this polar-

ization does not penetrate the system and is therefore not screened. Thus, $\tilde{Q}^{(2)}$ coincides with $\tilde{Q}^{s}$ [Eq. (A15)], and is given in Eq. (24) for the benefit of the reader.

APPENDIX B: COMPARISON WITH EARLIER WORK

In Ref. 11 a simple model for the nonlinear response of a centrosymmetric dielectric was developed, which lead to explicit analytic expressions for the nonlinear bulk and surface response functions in terms of the linear response. The model consists of a continuous distribution of polarizable entities, each of which responds nonlinearly to the gradient of the field as a forced harmonic oscillator. Although very crude, that model is a convenient first step for the analysis of real systems, as it permits the actual calculation of spectra from the knowledge of only $\epsilon(\omega)$, which can be obtained experimentally or through microscopic calculations. In the present section we employ that model to obtain definite expressions for the response of small spheres.

From Eqs. (12), (13) and (14) of Ref. 11 we obtain the bulk polarization

$$\vec{P}^{b}=\frac{n}{2e}\alpha_1\alpha_2(\nabla E^2-4\vec{E}\cdot\nabla\vec{E})+\frac{n}{2e}\alpha_1^2\vec{E}\cdot\nabla\vec{E}, \quad \text{(B1)}$$

where n is the number density of polarizable ''molecules'' within the bulk and $\alpha_w=\alpha(w\omega)$ is the linear polarizability of each one, related to the dielectric function through $\epsilon_w=1+4\pi n\alpha_w$. Comparing Eq. (B1) with Eq. (16) we identify

$$\gamma=\frac{n}{2e}\alpha_1\alpha_2 \quad \text{(B2)}$$

and

$$\delta'=\frac{n}{2e}\alpha_1(\alpha_1-4\alpha_2). \quad \text{(B3)}$$

Substituting Eqs. (B2) and (B3) in Eqs. (25), (26), (27), and (28), we obtain

$$\gamma^{e}=\frac{3}{8\pi ne}\frac{\epsilon_1-1}{(\epsilon_1+2)(2\epsilon_1+3)(\epsilon_2+2)}[5(\epsilon_1-2\epsilon_2+1)+(\epsilon_1-1)(2\epsilon_2 a+b+3\epsilon_2 f)]R^3, \quad \text{(B4)}$$

$$\gamma^{m}=\frac{\gamma^{e}}{2}-\frac{3}{16\pi ne}\frac{\epsilon_1-1}{(\epsilon_1+2)(\epsilon_2+2)}[(\epsilon_1-6\epsilon_2+5)+(\epsilon_1-1)(b-\epsilon_2 f)]R^3, \quad \text{(B5)}$$

$$\gamma^{q}=\frac{9}{4\pi ne}\frac{(\epsilon_1-1)^2}{(\epsilon_1+2)^2(2\epsilon_2+3)}(\epsilon_2 a+3b-\epsilon_2 f)R^3, \quad \text{(B6)}$$

and

$$\tilde{\gamma}^{q}=\frac{3}{8\pi ne}\left(\frac{\epsilon_1-1}{\epsilon_1+2}\right)^2(a+2f)R^3. \quad \text{(B7)}$$

We complete the expressions above by stating in our notation the values of a, b, and f corresponding to the model of Ref. 11,

$$a(\omega)=2([\epsilon_2-\epsilon_1][2\epsilon_1-\epsilon_2-\epsilon_1\epsilon_2]+[\epsilon_1]^2[1-\epsilon_2]\log[\epsilon_1/\epsilon_2])/[\epsilon_2-\epsilon_1]^2, \quad \text{(B8)}$$

$$b=-1, \quad \text{(B9)}$$

and

$$f=0. \quad \text{(B10)}$$

Our γ^{e} and γ^{q} [Eqs. (B4) and (B6)] are similar to those obtained for pure longitudinal fields, given by Eqs. (40) and (41) of Ref. 9. However, in Ref. 9 no account was taken of the polarization linearly induced within the interior of the sphere by the field originated at the surface nonlinear polarization. Thus, a factor of L_{12} is missing from the surface term of Eq. (40) and a factor L_{22} is missing from the surface term of Eq. (41) in Ref. 9. Furthermore, an additional factor of ϵ_2 multiplying the surface response functions a and f is also missing from Ref. 9. Therefore, Sec. II corrects an oversight in Ref. 9 and extends its results to small spheres made up of isotropic, homogeneous, and centrosymmetric materials with arbitrary bulk and surface response functions γ, δ', a, b, and f and excited by a field with both longitudinal and transverse components.

Another calculation similar to ours was performed in a recent work,[6,16] where the nonlinear response of a small sphere to a plane electromagnetic wave was studied. In Refs. 6 and 16 a magnetic response was allowed, the sphere was embedded within a polarizable medium and the surface response took place within a thin spherical shell that screened the surface polarization. Since $\vec{E}^{\mathrm{ex}}\cdot\nabla E^{\mathrm{ex}}$ vanishes for a plane electromagnetic wave, from the calculation by Dadap *et al.* it is only possible to extract values for γ^{m}, γ^{q} and $\tilde{\gamma}^{q}$. In our notation, Eqs. (12) of Ref. 16 become

$$\vec{p}^{(2)}=\frac{8\pi i}{15}R^3\chi_1\vec{q}(E^0)^2 \quad \text{(B11)}$$

and

$$\vec{\tilde{Q}}\cdot\hat{n}+\tilde{Q}\hat{n}=\frac{8\pi}{5}R^3[(\chi_1-5\gamma)\hat{n}(E^0)^2+2\chi_2\vec{E}^0\cdot\hat{n}\vec{E}^0], \quad \text{(B12)}$$

from which we identify

$$\gamma^{m}=\frac{8\pi}{15}R^3\chi_1, \quad \text{(B13)}$$

$$\gamma^{q}=\frac{16\pi}{5}R^3\chi_2, \quad \text{(B14)}$$

and

$$\tilde{\gamma}^{q}-\frac{\gamma^{q}}{3}=\frac{8\pi}{5}R^3(\chi_1-5\gamma). \quad \text{(B15)}$$

Here, χ_1 and χ_2 are parameters introduced in Ref. 16. Similar equations were presented in Ref. 6, but without the nonradiating radial term of Eq. (B12).

In the case we considered in Sec. II, the sphere is within vacuum and there is no magnetic response. Therefore, in our notation, Eqs. (22) of Ref. 16 reduce to

$$\chi_1=\frac{1}{4}L_{11}L_{12}\{5[(\delta'+2\gamma)L_{21}-(\delta'-2\gamma)] +2[(2\eta_2\eta_1^2\tilde{\chi}^s_{\perp\perp\perp}+\eta_1\tilde{\chi}^s_{\parallel\perp\parallel}+3\eta_2\tilde{\chi}^s_{\perp\parallel\parallel})L_{21} +5(\eta_2\tilde{\chi}^s_{\perp\parallel\parallel}-\eta_1\tilde{\chi}^s_{\parallel\perp\parallel})]\} \quad \text{(B16)}$$

and

$$\chi_2=L_{11}^2L_{22}(\eta_2\eta_1^2\tilde{\chi}^s_{\perp\perp\perp}+3\eta_1\tilde{\chi}^s_{\parallel\perp\parallel}-\eta_2\tilde{\chi}^s_{\perp\parallel\parallel}), \quad \text{(B17)}$$

where we denoted the surface susceptibility employed in Refs. 6 and 16 by $\tilde{\chi}^s_{ijk}$, defined through $\tilde{P}^s_i\equiv\tilde{\chi}_{ijk}E_jE_k$, where the electric field is evaluated within an interfacial layer[3] with dielectric function ϵ' which further screens the normal component of the surface polarization $\tilde{P}^s$. This definition differs in general from that of our susceptibility [Eq. (18)]. Here we introduced $\eta\equiv\epsilon/\epsilon'$. According to our definition of the surface susceptibility [Eq. (18)], the choice $\epsilon_1'=\epsilon_2'=1$ leads to $\tilde{\chi}^s_{ijk}=\chi^s_{ijk}$, so that substituting Eqs. (B16) and (B17) into Eqs. (B13) and (B14), and with the replacements

$$\eta_2\eta_1^2\tilde{\chi}^s_{\perp\perp\perp}\rightarrow\epsilon_2\chi^s a, \quad \eta_1\tilde{\chi}^s_{\parallel\perp\parallel}\rightarrow\chi^s b, \quad \eta_2\tilde{\chi}^s_{\perp\parallel\parallel}\rightarrow\epsilon_2\chi^s f, \quad \text{(B18)}$$

we recover our Eqs. (26) and (27). On the other hand,

$$\tilde{\gamma}^q=\frac{\gamma^q}{3}+3\gamma^m-8\pi R^3\gamma \quad \text{(B19)}$$

does not agree with our Eq. (28). This is not too important as the scalar second moment $\tilde{Q}^{(2)}$ does not radiate. Therefore, our results are also a generalization of those of Refs. 6 and 16 to small nonmagnetic spheres immersed in vacuum and excited by a field which is not necessarily a plane wave.

[1] H.W.K. Tom, T.F. Heinz, and Y.R. Shen, Phys. Rev. Lett. **51**, 1983 (1983); J.E. Sipe, D.J. Moss, and H.M. van Driel, Phys. Rev. B **35**, 1129 (1987); P. Guyot-Sionnest and Y.R. Shen, *ibid.* **38**, 7985 (1988); S. Janz and H.M. van Driel, Int. J. Nonlinear Opt. Phys. **2**, 1 (1993).

[2] G.A. Reider and T.F. Heinz, in *Photonic Probes of Surfaces*, edited by P. Halevi (Elsevier, Amsterdam, 1995), Chap. 9; J.E. McGilp, Surf. Rev. Lett. **6**, 529 (1999); G. Lüpke, Surf. Sci. Rep. **35**, 75 (1999); N. Bloembergen, Appl. Phys. B: Lasers Opt. **68**, 289 (1999); M.C. Downer, B.S. Mendoza, and V.I. Gavrilenko, Surf. Interface Anal. **31**, 966 (2001).

[3] T.F. Heinz, in *Nonlinear Surface Electromagnetic Phenomena*, edited by H.-E. Ponath and G.I. Stegeman (Elsevier, Amsterdam, 1991), p. 354.

[4] G.S. Agarwal and S.S. Jha, Solid State Commun. **41**, 499 (1982); X.M. Hua and J.I. Gersten, Phys. Rev. B **33**, 3756 (1986); D. Östling, P. Stampfli, and K.H. Bennemann, Z. Phys. D: At., Mol. Clusters **28**, 169 (1993); J. Martorell, R. Vilaseca, and R. Corbalán, Phys. Rev. A **55**, 4520 (1997).

[5] Y. Jiang, P.T. Wilson, M.C. Downer, C.W. White, and S.P. Withrow, Appl. Phys. Lett. **78**, 766 (2001).

[6] J.I. Dadap, J. Shan, K.B. Eisenthal, and T.F. Heinz, Phys. Rev. Lett. **83**, 4045 (1999).

[7] J.I. Dadap, J. Shan, and T.F. Heinz, in *Book of Abstracts, Adriatico Research Conference on Lasers in Surface Science* (International Centre for Theoretical Physics, Trieste, Italy, 2000) p. 38.

[8] N. Yang, W.E. Angerer, and A.G. Yodh, Phys. Rev. Lett. **87**, 103902 (2001).

[9] Vera L. Brudny, Bernardo S. Mendoza, and W. Luis Mochán, Phys. Rev. B **62**, 11152 (2000).

[10] W. Luis Mochán and Rubén G. Barrera, Phys. Rev. B **32**, 4984 (1985); **32**, 4989 (1985).

[11] Bernardo S. Mendoza and W. Luis Mochán, Phys. Rev. B **53**, 4999 (1996).

[12] R.H. Good, Jr. and T.J. Nelson, *Classical Theory of Electric and Magnetic Fields* (Academic, New York, 1971) Sec. 9.

[13] N. Bloembergen, R.K. Chang, S.S. Jha, and C.H. Lee, Phys. Rev. **174**, 813 (1968); **178**, 1528(E) (1969).

[14] J. Rudnick and E.A. Stern, Phys. Rev. B **4**, 4274 (1971).

[15] P. Guyot-Sionnest, A. Tadjeddine, and A. Liebsch, Phys. Rev. Lett. **64**, 1678 (1990).

[16] J.I. Dadap, J. Shan, K.B. Eisenthal, and T.F. Heinz (unpublished).

[17] G. Russakoff, Am. J. Phys. **38**, 1188 (1970).

[18] H. Kogelnik and T. Li, Appl. Opt. **5**, 1550 (1966).

[19] M. Downer (private communication).

[20] H. Wang, E.C.Y. Yan, E. Borguet, and K.B. Eisenthal, Chem. Phys. Lett. **259**, 15 (1996).

[21] D.E. Aspnes and A.A. Studna, Phys. Rev. B **27**, 985 (1983).

[22] J.D. Jackson, *Classical Electrodynamics*, 2nd. ed. (Wiley, New York, 1975), Chap. 4.